

Detection of slow slip events using wavelet analysis of GNSS recordings

Ariane Ducellier¹, Kenneth C. Creager¹, and David A. Schmidt¹

¹University of Washington, Department of Earth and Space Sciences, Box 351310, 4000 15th Avenue NE Seattle, WA 98195-1310

Key points

- 8 • We use a wavelet-based signal processing method to detect transients in
 - 9 GNSS data, such as slow slip events.
 - 10 • There is a good correlation between detections of slow slip using GNSS
 - 11 data and using tremor data.
 - 12 • The method could be applied in regions where no tremor are detected in
 - 13 conjunction with slow slip events.

14 Abstract

15 In many places, tectonic tremor is observed in relation to slow slip and can
16 be used as a proxy to study slow slip events of moderate magnitude where
17 surface deformation is hidden in Global Navigation Satellite System (GNSS)
18 noise. However, in subduction zones where no clear relationship between tremor
19 and slow slip occurrence is observed, these methods cannot be applied, and we
20 need other methods to be able to better detect and quantify slow slip. Wavelets
21 methods such as the Discrete Wavelet Transform (DWT) and the Maximal
22 Overlap Discrete Wavelet Transform (MODWT) are mathematical tools for
23 analyzing time series simultaneously in the time and the frequency domain by
24 observing how weighted differences of a time series vary from one period to the
25 next. In this paper, we use wavelet methods to analyze GNSS time series and
26 seismic recordings of slow slip events in Cascadia. We use detrended GNSS
27 data, apply the MODWT transform and stack the wavelet details over several
28 nearby GNSS stations. As an independent check on the timing of slow slip
29 events, we also compute the cumulative number of tremor in the vicinity of the
30 GNSS stations, detrend this signal, and apply the MODWT transform. In both
31 time series, we can then see simultaneous waveforms whose timing corresponds
32 to the timing of slow slip events. We assume that there is a slow slip event
33 whenever there is a positive peak followed by a negative peak in the wavelet
34 signal. We verify that there is a good correlation between slow slip events
35 detected with only GNSS data, and slow slip events detected with only tremor
36 data for northern Cascadia. The wavelet-based detection method detects well
37 events of magnitude higher than 6 as determined by independent event catalogs
38 (e.g. [Michel et al., 2019]).

39 1 Introduction

40 Slow slip events are a new feature discovered in the last two decades in many
41 subduction zones thanks to recordings of the displacement of Earth's surface by
42 dense Global Navigation Satellite System (GNSS) networks. As with ordinary
43 earthquakes, slow slip events represent slip on a fault, for instance the plate
44 boundary between a tectonic plate subducting under another tectonic plate.
45 However, they take a much longer time (several days to several years) to happen
46 relative to ordinary earthquakes. They have a relatively short recurrence
47 time (months to years) compared to the recurrence time of regular earthquakes
48 (up to several hundreds of years), allowing scientists to observe and study many
49 complete event cycles, which is typically not possible to explore with traditional
50 earthquake catalogs [Beroza and Ide, 2011]. A slow slip event on the plate
51 boundary is inferred to happen when there is a reversal of the direction of motion
52 at GNSS stations, compared to the secular interseismic motion. Slow slip
53 events have been observed in many places, such as Cascadia, Nankai (southwest
54 Japan), Alaska, Costa Rica, Mexico, and New Zealand [Beroza and Ide, 2011,
55 Audet and Kim, 2016].

56
57 In many places, tectonic tremor is also observed in relation to slow slip, but
58 it is more abundant in some places. Tremor is a long (several seconds to many
59 minutes), low amplitude seismic signal, with emergent onsets, and an absence
60 of clear impulsive phases. Tectonic tremor have been explained as a swarm of
61 small, low-frequency earthquakes (LFEs) [Shelly et al., 2007], which are small
62 magnitude earthquakes ($M \sim 1$) for which frequency content (1-10 Hz) is lower
63 than for ordinary earthquakes (up to 20 Hz). In subduction zones such as Nankai
64 and Cascadia, tectonic tremor observations are spatially and temporally corre-
65 lated with slow slip observations [Obara, 2002, Rogers and Dragert, 2003]. Due
66 to this correlation, these paired phenomena have been called Episodic Tremor
67 and Slip (ETS). However, this is not always the case. For instance, in northern
68 New Zealand, tremor are more challenging to detect, and seem to be located
69 downdip of the slow slip on the plate boundary [Todd and Schwartz, 2016]. In
70 Alaska, the tremor zone only partially overlaps the long-term slow slip zone and
71 there does not appear to be any temporal correlation between tremor and slow
72 slip occurrence [Wech, 2016].

73
74 In Cascadia, there are robust signals in both GNSS and tremor. This is
75 also the case in Nankai, where tiltmeters are used instead of GNSS. It is thus
76 possible to use tremor as a proxy to observe slow slip events that are not di-
77 rectly observed in the GNSS data. For instance, Aguiar et al. [2009] studied
78 23 ETS events in Cascadia with more than 50 hours of tectonic tremor. For
79 all these events, they computed both the GPS-estimated moment release and
80 the cumulative number of hours of tectonic tremor recorded. They observed a
81 linear relationship between moment release and number of hours of tremor for
82 ETS events of moment magnitude 6.3 to 6.8. Based on this linear relationship,
83 it is possible to infer the existence of smaller slow slip events of magnitude 5-6
84 occurring simultaneously with smaller tremor bursts of duration 1 to 50 hours
85 occurring in between the big ETS events, and for which there is no detectable
86 signal in the GPS data.

87
88 Frank [2016] divided GPS time series observations from Cascadia and Guer-
89 rero, Mexico, into two groups: the first group contains days with abundant
90 tremor and LFEs, the second group contains days when the number of tremor
91 or LFEs is lower than a threshold. He then stacked separately the two groups
92 of daily observations and observed a cumulative displacement in the direction
93 corresponding to the loading period when few tremor or LFEs are observed
94 and the surface deformation corresponds to the secular plate motion. He also
95 observed a cumulative displacement in the opposite direction corresponding to
96 the release period when tremor and LFEs are observed. He was thus able to
97 observe a reverse displacement corresponding to smaller slow slip events not
98 directly observable in the GPS data for individual events.

99
100 However, these methods cannot be applied to detect slow slip events in places
101 where tremor and slow slip occurrence are not well spatially and temporary cor-

102 related, tremor is not abundant, or the seismic network is not robust enough.
103 We thus need other methods to be able to better detect and quantify slow slip.

104

105 Wavelets methods such as the Discrete Wavelet Transform (DWT) are mathematical
106 tools for analyzing time series simultaneously in the time and the frequency domain by observing how weighted differences of a time series vary from
107 one period to the next. Wavelet methods have been widely used for geophysical
108 applications (e.g. [Kumar and Foufoula-Georgiou, 1997]). However, few studies
109 have used wavelet methods to analyze recordings of slow slip, and their scope
110 was limited to the detection of the bigger (magnitude 6-7) short-term (a few
111 weeks) events [Szeliga et al., 2008, Ohtani et al., 2010, Wei et al., 2012, Alba
112 et al., 2019].

114

115 Szeliga et al. [2008] determined the timing and the amplitude of 34 slow
116 slip events throughout the Cascadia subduction zone between 1997 and 2005
117 using wavelets. They modeled the GPS time series by the sum of a linear trend,
118 annual and biannual sinusoids representing seasonal effects, Heaviside step functions
119 corresponding to earthquakes and hardware upgrades, and a residual signal.
120 They then applied a Gaussian wavelet transform to the residual time series
121 to get the exact timing of slow slip at each GPS station. The idea is that the
122 wavelet transform allows us to analyze the signal both in the time and the frequency
123 domains. A sharp change in the signal will be localized and seen at all
124 levels of the wavelet decomposition, contrary to what happens with the periodic
125 sinusoids of the Fourier transform.

126

127 Instead of using wavelets in the time domain, Ohtani et al. [2010] used 2D
128 wavelet functions in the spatial domain to detect slow slip events. They de-
129 signed the Network Stain Filter (NSF) to detect transient deformation signals
130 from large-scale geodetic arrays. They modeled the position of the GPS station
131 by the sum of the secular velocity, a spatially coherent field, site-specific noise,
132 reference frame errors, and observation errors. The spatial displacement field is
133 modeled by the sum of basis wavelets with time-varying weights. Their method
134 has been successfully used to detect a transient event in the Boso peninsula,
135 Japan, and a slow slip event in the Alaska subduction zone [Wei et al., 2012].

136

137 Finally, Alba et al. [2019] used hourly water level records from four tide
138 gauges in the Juan de Fuca Straight and the Puget Sound to determine rela-
139 tive vertical displacements associated with ETS events between 1996 and 2011.
140 Their main idea is that the tidal level measured at a given gauge is the sum of
141 a noise component at multiple timescales (tides, ocean and atmospheric noise)
142 and an uplift signal due to the ETS events. The noise component is assumed to
143 be coherent between all tidal gauges, while the tectonic uplift signal is different
144 provided that the gauges are far enough from each other. By stacking the tidal
145 records after removing tides, the uplift signals cancel each other while the noise
146 signal is amplified. By stacking the details of the DWT decomposition, instead
147 of stacking the raw tidal record, each of the components of the noise at different

148 time scales is retrieved and can then be removed from the raw records to obtain
149 the uplift signal. The authors were then able to clearly see a difference in uplift
150 between the two tidal gauges at Port Angeles and Port Townsend.

151

152 In our study, we use a similar approach to previous studies with a different
153 reasoning. We only stack signals at nearby GPS stations, assuming that the
154 longitudinal displacement due to the ETS events will then be the same at each
155 of the GPS stations considered. We suppose that some of the noise component
156 is different at each GPS station and will be eliminated by the stacking. Fi-
157 nally, we assume that the noise and the longitudinal displacement due to the
158 ETS events and the secular plate motion have different time scales, so that the
159 wavelet decomposition will act as a bandpass filter to retrieve the displacement
160 signal and highlight the ETS events. We use wavelet methods to analyze GPS
161 and tremor recordings of slow slip events in Cascadia. Our objective is to verify
162 that there is a good correlation between slow slip events detected with only
163 GNSS data, and slow slip events detected with only tremor data. We thus want
164 to demonstrate that the wavelet-based detection method can be applied to de-
165 tect slow slip events that may currently be obscured using standard methods.

166

167 2 Data

168 We focused our study on northwest Washington State. For the GNSS data, we
169 used the GPS time series provided by the Pacific Northwest Geodetic Array,
170 Central Washington University. These are network solutions in ITRF2008 with
171 phase ambiguities resolved. Solutions are computed with JPL/NASA orbits and
172 satellite clocks. North, East, and Vertical directions are available. However, as
173 the direction of the secular plate motion is close to the East direction, we only
174 used the East direction of the GPS time series for the data analysis, as it has
175 the best signal-to-noise ratio. The wavelet method works best with data with
176 zero mean, and no sharp discontinuities; so we use the cleaned dataset, that is
177 GPS times series with linear trends, steps due to earthquakes or hardware up-
178 grades, and annual and semi-annual sinusoids signals simultaneously estimated
179 and removed following Szeliga et al. [2004]. For the tremor data, we used the
180 tremor catalog from the Pacific Northwest Seismic Network (PNSN) [Wech,
181 2010].

182

183 3 Method

184 3.1 The Maximal Overlap Discrete Wavelet Transform

185 The Discrete Wavelet Transform (DWT) is an orthonormal transform that
186 transforms a time series X_t ($t = 0, \dots, N - 1$) into a vector of wavelet coeffi-
187 cients W_i ($i = 0, \dots, N - 1$). If we denote J the level of the wavelet decompo-

188 sition, and the number of observations is equal to $N = n * 2^J$, where n is some
 189 integer higher or equal to 1, the vector of wavelet coefficients can be decomposed
 190 into J wavelet vectors W_j of lengths $\frac{N}{2}, \frac{N}{4}, \dots, \frac{N}{2^J}$, and one scaling vector V_J
 191 of length $\frac{N}{2^J}$. Each wavelet vector W_j is associated with changes on time scale
 192 $\tau_j = dt2^{j-1}$, where dt is the time step of the time series, and corresponds to the
 193 filtering of the original time series with a filter with nominal frequency interval
 194 $[\frac{1}{dt2^{j+1}}; \frac{1}{dt2^j}]$. The scaling vector V_J is associated with averages in time scale
 195 $\lambda_J = dt2^J$, and corresponds to the filtering of the original time series with a
 196 filter with nominal frequency interval $[0; \frac{1}{dt2^{j+1}}]$. Wavelet vectors can be further
 197 decomposed into details and smooths, which are more easily interpretable. We
 198 define for $j = 1, \dots, J$ the j th wavelet detail D_j , which is a vector of length
 199 N , and is associated to time scale $\tau_j = dt2^{j-1}$. Similarly, we can define for
 200 $j = 1, \dots, J$ the j th wavelet smooth S_j , which is a vector of length N , and is
 201 associated to scales $\tau_{j+1} = dt2^{j+1}$ and higher. The basic idea is to reapply to
 202 W_j the wavelet filter that was used to construct W_j from the initial time series
 203 X . Together, the details and the smooths define the multiresolution analysis
 204 (MRA) of X :

$$205 \quad X = \sum_{j=1}^J D_j + S_J \quad (1)$$

206 The DWT presents several disadvantages. First, the length of the time se-
 207 ries must be a multiple of 2^J where J is the level of the DWT decomposition.
 208 Second, the time step of the wavelet vector W_j is $dt2^j$, which may not corre-
 209 spond to the time when some interesting phenomenon is visible on the original
 210 time series. Third, when we circularly shift the time series, the corresponding
 211 wavelet coefficients, details and smooths are not a circularly shifted version of
 212 the wavelet coefficients, details and smooths of the original time series. Thus,
 213 the values of the wavelet coefficients, details and smooths are strongly dependent
 214 on the time when we start experimentally gathering the data. Finally, when we
 215 filter the time series to obtain the details D_j and smooths S_j , we introduce a
 216 phase shift, which makes it difficult to line up meaningfully the features of the
 217 MRA with the original time series.

218 To overcome the disadvantages described above, we use instead the Maxi-
 219 mal Overlap Discrete Wavelet Transform (MODWT). The MODWT transforms
 220 the time series X_t ($t = 0, \dots, N - 1$) into J wavelet vectors \tilde{W}_j ($j = 1, \dots, J$) of
 221 length N and a scaling vector \tilde{V}_J of length N . As is the case for the DWT,
 222 each wavelet vector \tilde{W}_j is associated with changes on scale $\tau_j = dt2^{j-1}$, and
 223 corresponds to the filtering of the original time series with a filter with nominal
 224 frequency interval $[\frac{1}{dt2^{j+1}}; \frac{1}{dt2^j}]$. The scaling vector \tilde{V}_J is associated with aver-
 225 ages in scale $\lambda_J = dt2^J$, and corresponds to the filtering of the original time
 226 series with a filter with nominal frequency interval $[0; \frac{1}{dt2^{j+1}}]$. As is the case for
 227 the DWT, we can write the MRA:

$$X = \sum_{j=1}^J \tilde{D}_j + \tilde{S}_J \quad (2)$$

230 The MODWT of a time series can be defined for any length N . The time
 231 step of the wavelet vectors \tilde{W}_j and the scaling vector \tilde{V}_J is equal to the time
 232 step of the original time series. When we circularly shift the time series, the
 233 corresponding wavelet vectors, scaling vector, details and smooths are shifted
 234 by the same amount. The details and smooths are associated with a zero phase
 235 filter, making it easy to line up meaningfully the features of the MRA with the
 236 original time series. The wavelet methods for time series analysis are explained
 237 in a more detailed way in [Percival and Walden, 2000]).

238

239 3.2 Application to synthetic data

240 To illustrate the wavelet transform method, we first apply the MODWT to syn-
 241 thetic data. As slow slip events occur in Cascadia on a regular basis, every
 242 twelve to eighteen months, we create a synthetic signal of period $T = 500$ days.
 243 To reproduce the ground displacement observed on the longitudinal component
 244 of GPS stations in Cascadia, we divide each period into two parts: In the first
 245 part of duration $T - N$, the displacement is linearly increasing and corresponds
 246 to the inter seismic plate motion in the eastern direction; in the second part
 247 of duration N , the displacement is linearly decreasing and corresponds to a
 248 slow slip event on a reverse fault at depth triggering a ground displacement in
 249 the western direction. To see the effect of the duration of the slow slip event,
 250 we use different values for $N = 5, 10, 20, 40$ days. The amplitude of the set is
 251 normalized to 1. Figure 1 shows the synthetics, the details D_j of the wavelet
 252 decomposition for levels 1 to 10, and the smooth S_{10} for the four durations of a
 253 slow slip event.

254

255 The ramp-like signal is transformed through the wavelet filtering into a wave-
 256 form with first a positive peak and then a negative peak. The shape of the wave-
 257 form is the same for every level of the wavelet decomposition, but the width of
 258 the waveform increases with the scale level. For the 8th level of the wavelet de-
 259 composition, the width of the waveform is nearly as large as the time between
 260 two events. At larger scales, the waveforms start to merge two contiguous events
 261 together, and make the wavelet decomposition less interpretable. For an event
 262 of duration 5 days, the wavelet details at levels higher than 3 have a larger
 263 amplitude than the wavelet details at lower scales. For an event of duration 10
 264 days, the wavelet details at levels higher than 4 have a larger amplitude than
 265 the wavelet details at lower scales. For an event of duration 20 days, the wavelet
 266 details at levels higher than 5 have a larger amplitude than the wavelet details
 267 at lower scales. For an event of duration 40 days, the wavelet details at levels
 268 higher than 6 have a larger amplitude than the wavelet details at lower scales.
 269 Thus, the scale levels at which an event is being seen in the wavelet details give

270 us an indication about the duration (and the magnitude) of the slow slip event.
271 The big slow slip events of magnitude 6-7 typically trigger a signal that lasts
272 about one week at an individual GPS station, and the whole event lasts several
273 weeks. We expect them to start being visible at the level 5 of the wavelet de-
274 composition, but to not be noticeable at lower time scales.

275

276 3.3 MODWT of GPS and tremor data

277 The DWT and MODWT methods must be used on a continuous time series,
278 without gaps in the recordings. To deal with the gaps in the GNSS recordings,
279 we simply replace the missing values by interpolation. The value for the first
280 day for which data are missing is equal to the mean of the five days before
281 the gap. The value for the last day for which data are missing is equal to the
282 mean of the five days after the gap. The remaining missing values are com-
283 puted by doing a linear interpolation of the first and the last values and adding
284 a Gaussian noise component with mean zero and standard deviation equal to
285 the standard deviation of the whole time series. The straight line starts at and
286 ends at . We verify how the wavelet details may be affected by looking at a GPS
287 time series without missing values and compared the wavelet details with and
288 without removing some data points. Station PGC5 recorded continuous 1390
289 days between 2009 and 2013 without any missing values. We first computed
290 the wavelet details without missing values. Then, we removed ten neighboring
291 values, replaced them using the method described above (linear interpolation
292 plus Gaussian noise), and computed the wavelet details with the replaced val-
293 ues. Figure 2 shows a comparison of the two wavelet details for two different
294 locations of the missing values. We can see that there are visible differences
295 in the time series itself, and in the details at the smallest levels of the wavelet
296 decomposition. However, the differences between the wavelet details with and
297 without missing values get smaller and smaller with increasing levels of details,
298 and are barely visible for the levels that are most relevant (levels 6 and above).
299 We thus conclude that we can easily replace the missing values in the GNSS
300 time series without introducing false detections of slow slip events.

301

302 We then applied the wavelet filtering to real GPS data. Figure 3 shows the
303 longitudinal displacement for GPS station PGC5, located in southern Vancou-
304 ver Island, the details of the wavelet decomposition for levels 1 to 8, and the
305 smooth. In the data, we can see a sharp drop in displacement whenever there is
306 a documented slow slip event. For levels 5 to 8, which correspond to time scales
307 16, 32, 64 and 128 days, we can see in the details a positive peak followed by
308 a negative peak whenever there is a drop in displacement in the data. We thus
309 verify that the wavelet method can detect steps in the time series associated
310 with slow slip events.

311

312 To increase the signal-to-noise ratio and better detect slow slip events, we
313 stack the signal from several neighboring GPS stations. We choose to focus on

314 GPS stations located close enough to the tremor zone to get a sufficiently high
315 amplitude of the slow slip signal. We choose 16 points along the 40 km depth
316 contour of the plate boundary (model from Preston et al. [2003]) with spacing
317 equal 0.1 degree in latitude (red triangles on Figure 4). Then we took all the
318 GPS stations located in a 50 km radius for a given point, compute the wavelet
319 details for the longitudinal displacement of each station, and stack each detail
320 over the GPS stations. We thus have a stacked detail for each level 1 to 10 of
321 the wavelet decomposition.

322

323 To assess the success of the wavelet decomposition for detecting slow slip
324 events in GPS time series, we validate the approach by comparing to an inde-
325 pendent proxy for ETS events. We took all the tremor epicenters located within
326 a 50 km radius centered on one of the 16 locations marked by red triangles on
327 Figure 3. Then we computed the cumulative number of tremor within this
328 circle. Finally, we removed a linear trend from the cumulative tremor count,
329 and applied the wavelet transform. Figure 5 shows an example of the wavelet
330 decomposition for the third northernmost location on Figure 4 (which is closest
331 to GPS station PGC5). Contrary to what happens for the GPS data, we see
332 a sharp increase in the time series whenever there is a tremor episode, which
333 translates into a negative peak followed by a positive peak in the wavelet details.

334

4 Results

335 We stacked the 8th level detail of the wavelet decomposition of the displacement
336 over all the GPS stations located in a 50 km radius of a given point, for the 16
337 locations indicated in Figure 3. The result is shown in the top panel of Figure 6,
338 where each line represents one of the locations along strike. To better highlight
339 the peaks in the wavelet details, we highlighted in red the time intervals where
340 the amplitude of the stacked detail is higher than a threshold, and in blue the
341 time intervals where the amplitude of the stacked detail is lower than minus the
342 threshold. To compare the GPS signal with the tremor signal, we plotted the
343 8th level detail of the wavelet decomposition of the tremor count on the bottom
344 panel of Figure 6. We multiplied by -1 the cumulative tremor count for the
345 wavelet decomposition in order to be able to match positive peaks with positive
346 peaks and negative peaks with negative peaks. In the tremor catalog from the
347 PNSN, there are 17 tremor events with more than 150 hours of tremor recorded.
348 The events are summarized in Table 1. The time of the event is the start date
349 plus half the duration of the event.

350

351 Although the latitudinal extension of the events is not always the same for
352 the GPS data and for the tremor data, we identify the same 13 events in both 8th
353 wavelet decompositions for the 8th level: January 2007, May 2008, May 2009,
354 August 2010, August 2011, September 2012, September 2013, August-November
355 2014, January 2016, March 2017, June 2018, March-November 2019, and Oc-
356 tober 2020-January 2021. Although there are two events in the tremor catalog

357 in August 2014 and November 2014, these two events are not distinguishable in
358 the 8th level details and look more like a single event slowly propagating from
359 South to North. The same phenomenon is observed in 2019 when two tremor
360 events in March and November 2019 are merged into a single event propagating
361 slowly from South to North. In 2020-2021, the wavelet decomposition of the
362 tremor shows one event in the south in October–November 2020 and one event
363 in the North in January 2021, but in the wavelet decomposition of the GPS
364 data, these three events look like a single event propagating slowly from South
365 to North.

366

367 A similar comparison is shown for the wavelet decomposition of the GPS
368 data and the wavelet decomposition of the tremor count data for the 7th level
369 and the 6th level respectively (Figures 7 and 8). The events are harder to see in
370 the 7th level than in the 8th level, both for the GPS data and the tremor count
371 data. The wavelet decomposition is more noisy for the GPS data between 2010
372 and 2012, but it does not seem that there are more slow slip events visible in
373 the 7th level.

374

375 For the 6th level detail, we see an additional event in the South in Fall 2009
376 that is present both in the GPS and the tremor data. It may correspond to the
377 northern extent of a big ETS event occurring in Fall 2009 south of the study
378 area (event 19 in the Michel et al. [2019] catalog). There are three small sig-
379 nals in the GPS data in Winter 2012, Fall 2017, and Winter 2020 that are not
380 present in the tremor data, and may be false detections. To summarize, we
381 assume that true detections are events present in both GPS and tremor time
382 series, and false detections are events present in the GPS but not in the tremor
383 time series. Then, all the 13 events present on the 8th level detail of the wavelet
384 decomposition are true detections and 14 of the 17 events present on the 6th
385 level detail of the wavelet decomposition are true detections.

386

387 5 Discussion

388 To better evaluate the number of true and false detections, we convert the
389 wavelet details into binary time series. If the absolute value of the wavelet
390 detail is higher than a threshold, we replace the value by 1 (for positive values)
391 or -1 (for negative values), otherwise we replace the value by 0. We do this
392 on both the wavelet details of the GPS data and of the tremor data. Then we
393 decide that if both the GPS and the tremor time series take the value 1 (or
394 both take the value -1), we have a true detection (true positive, TP). If the
395 GPS and the tremor time series have opposite signs, or if the absolute value of
396 the GPS time series is 1 but the value of the tremor time series is 0, we have a
397 false detection (false positive, FP). If both time series take the value 0, we do
398 not have detection (true negative, TN). If the GPS time series take the value
399 0, but the absolute value of the tremor time series is 1, we miss a detection

400 (false negative, FN). We then define the sensitivity (true positive rate) and the
 401 specificity (equal to 1 minus the false positive rate) as:

$$\begin{aligned} \text{sensitivity} &= \frac{TP}{TP + FN} \\ \text{specificity} &= \frac{TN}{TN + FP} \end{aligned} \quad (3)$$

402 We can then evaluate the quality of the detections obtained with our method
 403 by plotting a receiver operating characteristic curve (ROC curve). The ROC
 404 curve is widely used for binary classification problems in statistics and machine
 405 learning. We calculate an ROC value by varying the values of the threshold
 406 (here the two thresholds used to convert the GPS and the tremor time series
 407 into binary time series), computing the corresponding values of the true positive
 408 rate and the false positive rate (equal to 1 minus the specificity), and plotting
 409 the true positive rate as a function of the false positive rate. If the classifica-
 410 tion was made randomly, all the points would fall on the first diagonal. If the
 411 classifier was perfect, the corresponding point would fall on the top left cor-
 412 ner of the graph with true positive rate equal to 1 and false positive rate equal
 413 to 0. The bigger the area under the curve, the better the classification method is.

414
 415 As the slow slip events are better seen on levels 6, 7 and 8 of the wavelet
 416 decomposition, we first add the wavelet details corresponding to levels 6 to 8,
 417 and transform the resulting time series into a binary time series. We apply this
 418 transform to both the GPS and the tremor time series with varying thresholds.
 419 We then plot the ROC curve on Figure 9, each dot representing a different
 420 threshold. The corresponding sums of the wavelet details for the GPS data and
 421 the tremor data are shown on Figure 10. We can see that there is a trade-off
 422 between sensitivity and specificity as we vary the threshold. If we decrease the
 423 false positive rate, we also decrease the number of true events detected. If we
 424 increase the number of true events detected, we also increase the false positive
 425 rate. In Figure 10, we have chosen thresholds for the GPS time series and the
 426 tremor time series such that the specificity is higher than 0.75, and the sensitiv-
 427 ity is the highest possible, that is we have chosen the thresholds corresponding
 428 to the dot that is farthest from the diagonal, which is random.

429
 430 In addition to the magnitude 6 events discussed above, Michel et al. [2019]
 431 have also identified several magnitude 5 events using a variational Bayesian In-
 432 dependent Component Analysis (vbICA) decomposition of the signal. As we
 433 expect smaller magnitude events to be more visible at smaller time scales of
 434 the wavelet decomposition (level 5), we verify for all these events whether a
 435 signal can be seen at the same time as the time given in their catalog. Most
 436 of these magnitude 5 events are also sub-events of bigger magnitude 6 events.
 437 Table 2 summarizes for each event its timing, its number and its magnitude as
 438 indicated in the catalog from Michel et al. [2019], and whether it is part of a
 439 bigger magnitude 6 event. Figure 11 shows the 5th level detail wavelet decom-
 440 position of the GPS data. Red lines show the timing of the big ETS events from

441 Table 1, and blue lines show the timing of the small slow slip events from Table 2.

442

443 All 14 events that are sub-events of a bigger event are visible at level 5.
444 However, this may be because the bigger events are clearly seen at levels 6 to 8,
445 and also at smaller time scales. The one small event that is not part of a bigger
446 event (Winter 2009) is visible at level 5 of the wavelet decomposition. However,
447 some other events that are not in the catalog of Michel et al. [2019]’s catalog
448 are also visible in late 2007, early 2010, early 2012, and late 2016. Therefore,
449 it is difficult to differentiate between a true detection and a false detection, and
450 to conclude whether the method can indeed detect events of magnitude 5.

451

452 In Figure 9, we see four smaller events that are not in the catalog of Michel
453 et al. [2019]: at about 2007.5, there is a negative peak followed by a positive peak
454 (that is an event in the opposite direction of what would be expected from slow
455 slip), at about 2010.2, 2012.2 and 2020.2, there are positive peaks followed by
456 negative peaks for all the sixteen locations studied in this paper. Looking back
457 at the original GPS data, there is a small increase in the displacement in the
458 eastern direction that lasts about one or two months at about 2007.5. However,
459 the direction of the displacement does not correspond to a slow slip event, and
460 another cause should be found to explain this signal. There is a decrease in
461 displacement that lasts several months at about 2010.2. This transient may
462 correspond to a long duration slow slip event. There is a small decrease in
463 displacement at about 2012.2. Its amplitude is small but the duration and
464 direction correspond to a slow slip event, so this transient could be a very small
465 slow slip event. Finally, there is also a small decrease in displacement at about
466 2020.2 that is difficult to interpret.

467

6 Conclusion

468 In this paper, we develop and test a new approach for detecting transient events
469 in GPS time series, such as slow slip events. We used wavelet methods to an-
470alyze GNSS time series and tremor recordings of slow slip events in Cascadia.
471 We used detrended GNSS data, applied the MODWT transform, and stacked
472 the wavelet details over several nearby GNSS stations. As an independent check
473 on the timing of slow slip events, we also computed the cumulative number of
474 tremor in the vicinity of the GNSS stations, detrended this signal, and applied
475 the MODWT transform. In both time series, we could then see simultaneous
476 waveforms whose timing corresponds to the timing of slow slip events. We as-
477 sumed that there is a slow slip event whenever the wavelet signal gets above
478 a threshold. We verified that there is a good correlation between slow slip
479 events detected with only GNSS data, and slow slip events detected with only
480 tremor data. The wavelet-based detection method detects all events of magni-
481 tude higher than 6 as determined by independent event catalogs (e.g. [Michel
482 et al., 2019]). We detected signals in the GPS data that could be magnitude
483 5 events, but it is not easy to differentiate between true detections and false

484 detections.

485 Data and Resources

486 The GPS recordings used for this analysis can be downloaded from the PANGA
487 website [GPS/GNSS Network and Geodesy Laboratory: Central Washington
488 University, other/seismic network, 1996] <http://www.panga.cwu.edu/>. The
489 Python scripts used to analyze the data and make the figures can be found
490 on the first author's Github account [https://github.com/ArianeDucellier/
491 slowslip](https://github.com/ArianeDucellier/slowslip). Figure 4 was created using GMT [Wessel and Smith, 1991].

492 Acknowledgements

493 This work was funded by the grant from the National Science Foundation EAR-
494 1358512. A.D. would like to thank Professor Donald Percival for introducing
495 her to wavelet methods during his excellent class on Wavelets: Data Analysis,
496 Algorithms and Theory taught at University of Washington.

497 Declaration of Competing Interests

498 The authors declare no competing interests.

499 References

- 500 A.C. Aguiar, T.I. Melbourne, and C.W. Scrivner. Moment release rate of Cas-
501 cadia tremor constrained by GPS. *Journal of Geophysical Research*, 114:
502 B00A05, 2009.
- 503 S. Alba, R. J. Weldon, D. Livelybrooks, and D. A. Schmidt. Cascadia ETS
504 events seen in tidal records (1980–2011). *Bulletin of the Seismological Society
505 of America*, 2019.
- 506 P. Audet and Y.H. Kim. Teleseismic constraints on the geological environment
507 of deep episodic slow earthquakes in subduction zone forearcs: A review.
508 *Tectonophysics*, 670:1–15, 2016.
- 509 G.C. Beroza and S. Ide. Slow earthquakes and nonvolcanic tremor. *Annual
510 Review of Earth and Planetary Sciences*, 39:271–296, 2011.
- 511 W.B. Frank. Slow slip hidden in the noise: The intermittence of tectonic release.
512 *Geophysical Research Letters*, 43:10125–10133, 2016.
- 513 GPS/GNSS Network and Geodesy Laboratory: Central Washington University,
514 other/seismic network. Pacific Northwest Geodetic Array (PANGA), 1996.
515 URL <http://www.panga.cwu.edu/>.

- 516 P. Kumar and E. Foufoula-Georgiou. Wavelet analysis for geophysical applica-
517 tions. *Reviews of Geophysics*, 35(4):385–412, 1997.
- 518 S. Michel, A. Gualandi, and J.-P. Avouac. Interseismic coupling and slow slip
519 events on the Cascadia megathrust. *Pure and Applied Geophysics*, 176:3867–
520 3891, 2019.
- 521 K. Obara. Nonvolcanic deep tremor associated with subduction in southwest
522 Japan. *Science*, 296(5573):1679–1681, 2002.
- 523 R. Ohtani, J.J. McGuire, and P. Segall. Network strain filter: A new tool
524 for monitoring and detecting transient deformation signals in GPS arrays.
525 *Journal of Geophysical Research*, 115:B12418, 2010.
- 526 D.B. Percival and A.T. Walden. *Wavelet Methods for Time Series Analysis*.
527 Cambridge Series in Statistical and Probabilistic Mathematics. Cambridge
528 University Press, New York, NY, USA, 2000.
- 529 L.A. Preston, K.C. Creager, R.S. Crosson, T.M. Brocher, and A.M. Trehu.
530 Intraslab earthquakes: Dehydration of the Cascadia slab. *Science*, 302:1197–
531 1200, 2003.
- 532 G. Rogers and H. Dragert. Tremor and slip on the Cascadia subduction zone:
533 The chatter of silent slip. *Science*, 300(5627):1942–1943, 2003.
- 534 D.R. Shelly, G.C. Beroza, and S. Ide. Non-volcanic tremor and low-frequency
535 earthquake swarms. *Nature*, 446:305–307, 2007.
- 536 W. Szeliga, T.I. Melbourne, M.M. Miller, and V.M. Santillan. Southern Cas-
537 cadia episodic slow earthquakes. *Geophysical Research Letters*, 31:L16602,
538 2004.
- 539 W. Szeliga, T. Melbourne, M. Santillan, and M. Miller. GPS constraints on 34
540 slow slip events within the Cascadia subduction zone, 1997–2005. *Journal of*
541 *Geophysical Research*, 113:B04404, 2008.
- 542 E.K. Todd and S.Y. Schwartz. Tectonic tremor along the northern Hikurangi
543 Margin, New Zealand, between 2010 and 2015. *Journal of Geophysical Re-*
544 *search Solid Earth*, 121:8706–8719, 2016.
- 545 A.G. Wech. Interactive tremor monitoring. *Seismological Research Letters*, 81
546 (4):664–669, 2010.
- 547 A.G. Wech. Extending Alaska’s plate boundary; tectonic tremor generated by
548 Yakutat subduction. *Geology*, 44(7):587–590, 2016.
- 549 M. Wei, J.J. McGuire, and E. Richardson. A slow slip event in the south central
550 Alaska Subduction Zone. *Geophysical Research Letters*, 39:L15309, 2012.
- 551 P. Wessel and W. H. F. Smith. Free software helps map and display data. *EOS*
552 *Trans. AGU*, 72:441, 1991.

553 **Addresses**

554 Ariane Ducellier. University of Washington, Department of Earth and Space
555 Sciences, Box 351310, 4000 15th Avenue NE Seattle, WA 98195-1310.

556 Kenneth C. Creager. University of Washington, Department of Earth and
557 Space Sciences, Box 351310, 4000 15th Avenue NE Seattle, WA 98195-1310.

559 David A. Schmidt. University of Washington, Department of Earth and
560 Space Sciences, Box 351310, 4000 15th Avenue NE Seattle, WA 98195-1310.
561

⁵⁶² **Tables**

Table 1: Episodic Tremor and Slip events with $M \geq 6$ identified by MODWT in both the GPS and the tremor data. The duration and the number of tremor are from the tremor catalog of the PNSN. The event number and the magnitude are from the slow slip catalog of Michel et al. [2019].

Time	Duration (days)	Number of tremor (hours)	Event number	Magnitude
2007.06	28	398	3	6.68
2008.36	25	402	10	6.56
2009.35	24	248	16	6.49
2010.63	29	518	24	6.54
2011.60	37	479	30	6.47
2012.72	37	620	34	6.54
2013.71	27	423	41	6.58
2014.65	15	190	48	6.03
2014.89	38	385	51	6.40
2016.11	43	421	54	6.79
2017.23	19	279	59	6.61
2018.49	22	381		
2019.23	34	195		
2019.88	16	205		
2020.79	26	193		
2020.86	12	162		
2021.09	14	230		

Table 2: Magnitude 5 events from Michel et al. [2019].

Time	Event number	Magnitude	Sub-event of bigger event
2007.06	1	5.64	Yes
2007.08	2	5.91	Yes
2008.38	11	5.50	Yes
2009.16	14	5.50	No
2009.36	17	5.32	Yes
2010.63	25	5.76	Yes
2011.66	31	5.61	Yes
2011.66	32	5.32	Yes
2012.69	35	5.56	Yes
2013.74	42	5.71	Yes
2014.69	49	5.31	Yes
2014.93	52	5.39	Yes
2016.03	57	5.80	Yes
2017.13	60	5.43	Yes
2017.22	61	5.37	Yes

563 **Figure captions**

- 564 • Figure 1. Demonstration of a wavelet decomposition for a synthetic dataset.
565 A synthetic time series is created (top row) with steps of period 500 days,
566 and transient durations of 2 days (left), 5 days, 10 days, and 20 days
567 (right). The resulting details and smooths are shown in increasing level.
568 The amplitude of the synthetic time series is normalized to 1, and the
569 details and smooths show the relative amplitude.
- 570 • Figure 2. Top: Data from GPS station PGC5 without missing values
571 (black) and with missing values replaced by the sum of a straight line and
572 a Gaussian noise component (red) for two locations of the missing values
573 (left and right). The corresponding ten details and smooths of the wavelet
574 composition are shown in increasing levels for the original data (black) and
575 for the missing values replaced by linear interpolation plus Gaussian noise
576 (red).
- 577 • Figure 3. Top: Longitudinal displacement recorded at GPS station PGC5.
578 The resulting details and smooth of the wavelet decomposition are shown
579 in increasing level.
- 580 • Figure 4. GPS stations used in this study (black triangles). The black
581 line represents the 40 km depth contour of the plate boundary model by
582 Preston et al. [2003]. The red triangles are the locations where we stack
583 the GPS data. The small grey dots are all the tremor locations from the
584 PNSN catalog.
- 585 • Figure 5. Details and smooth of the wavelet decomposition of the de-
586 trended cumulative tremor count around the third northernmost red tri-
587 angles on Figure 3 (latitude 48.5).
- 588 • Figure 6. Top: Stacked 8th level details of the wavelet decomposition of
589 the displacement over all the GPS stations located in a 50 km radius of a
590 given point, for the 16 red triangles indicated in Figure 3. Bottom: 8th
591 level detail multiplied by -1 of the cumulative tremor count in a 50 km
592 radius of a given point for the same 16 locations. The black lines represent
593 the timings of the ETS events from Table 1. We mark by a red rectangle
594 every time where the amplitude is higher than a threshold of 0.4 (for the
595 GPS) or 0.003 (for the tremor). We mark by a blue rectangle every time
596 where the amplitude is lower than minus the threshold.
- 597 • Figure 7. Same as Figure 6 but for the 7th level detail. The thresholds
598 are 0.5 (for the GPS) and 0.01 (for the tremor).
- 599 • Figure 8. Same as Figure 6 but for the 6th level detail. The thresholds
600 are 0.3 (for the GPS) and 0.009 (for the tremor).
- 601 • Figure 9. Same as Figure 6 but for the sum of the 6th, 7th and 8th level
602 details. The thresholds are 0.8 (for the GPS) and 0.01 (for the tremor).

- 603 • Figure 10. ROC curve for the sum of the 6th, 7th, and 8th level details
604 of the wavelet decomposition. Each black dot represents the true positive
605 rate of event detections and the false positive rate of event detections for
606 a given pair of thresholds (for the GPS and for the tremor). The red cross
607 marks the true positive rate and the false positive rate obtained with the
608 thresholds used to make Figure 9.
- 609 • Figure 11. Top: Stacked 5th level details of the wavelet decomposition
610 of the displacement over all the GPS stations located in a 50 km radius
611 of a given point, for the 16 red triangles indicated in Figure 3. The red
612 lines represent the timings of the ETS events from Table 1. The blue
613 lines represent the timings of the magnitude 5 events from the catalog of
614 Michel et al. [2019].

615 **Figures**

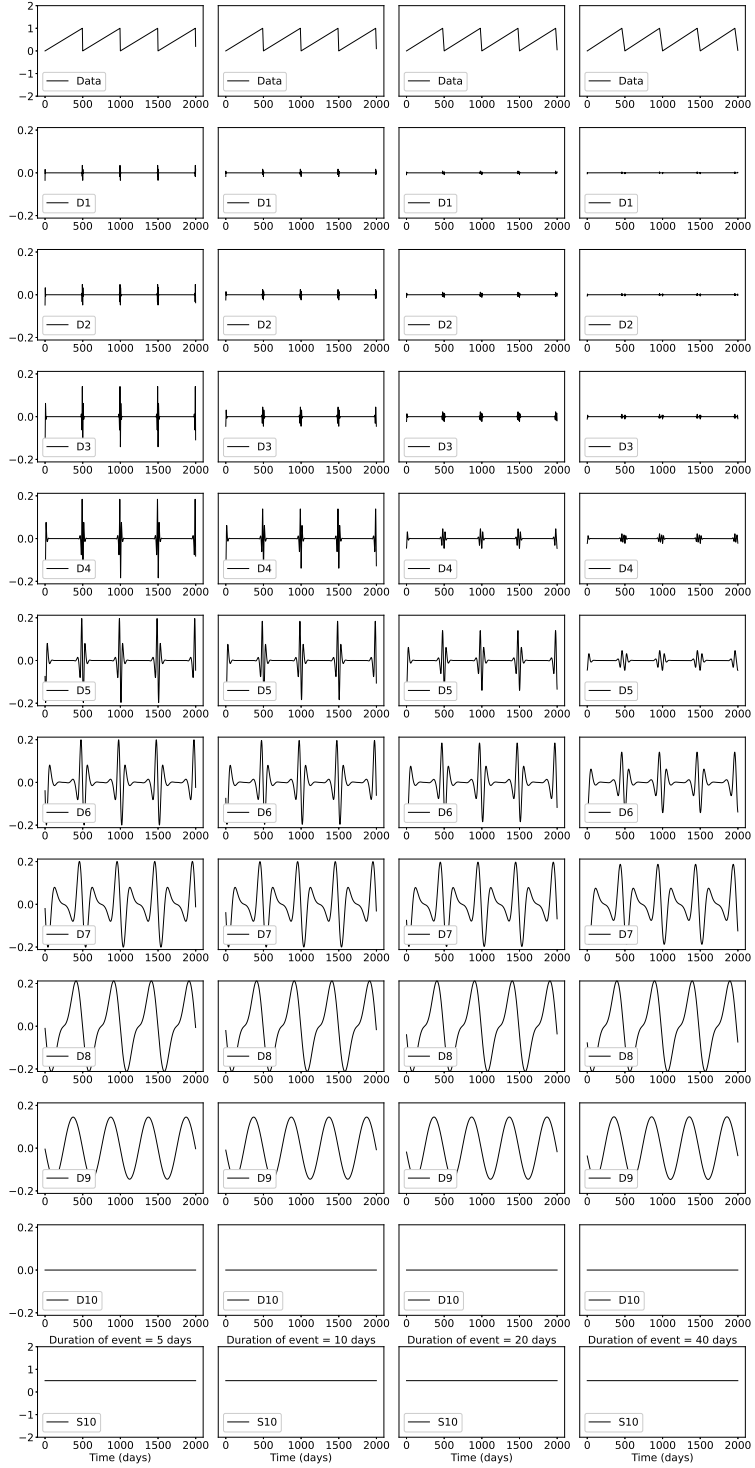


Figure 1: Demonstration of a wavelet decomposition for a synthetic dataset. A synthetic time series is created (top row) with steps of period 500 days, and transient durations of 2 days (left), 5 days, 10 days, and 20 days (right). The resulting details and smooths are shown in increasing level. The amplitude of the synthetic time series is normalized to 1, and the details and smooths show the relative amplitude.

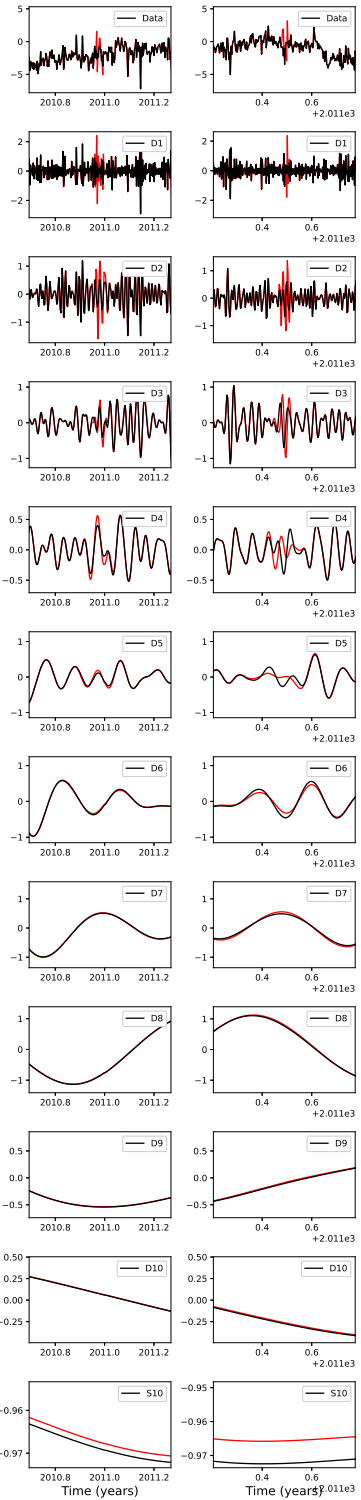


Figure 2: Top: Data from GPS station PGC5 without missing values (black) and with missing values replaced by the sum of a straight line and a Gaussian noise component (red) for two locations of the missing values (left and right). The corresponding ten details and smooths of the wavelet composition are shown in increasing levels for the original data (black) and for the missing values replaced by linear interpolation plus Gaussian noise (red).

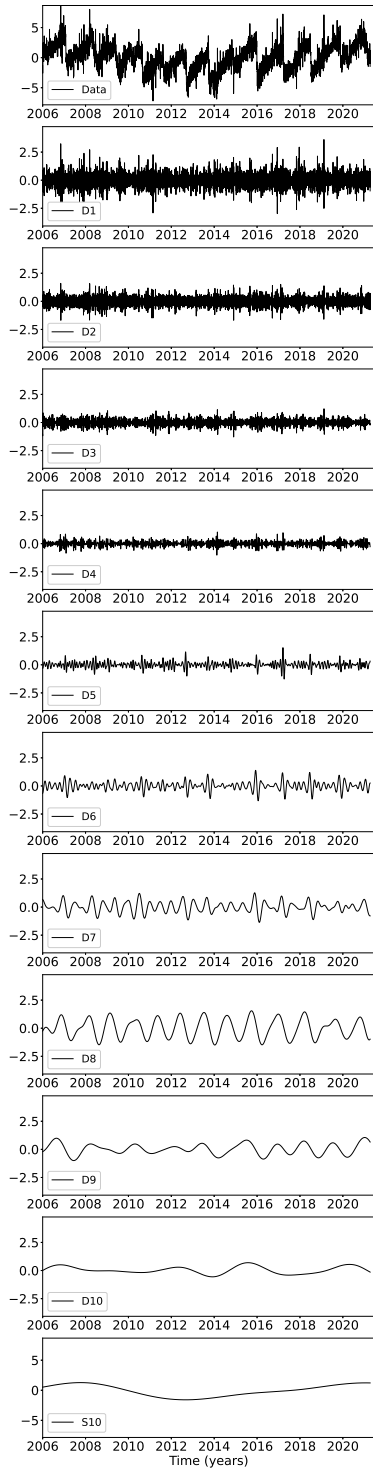


Figure 3: Top: Longitudinal displacement recorded at GPS station PGC5. The resulting details and smooth of the wavelet decomposition are shown in increasing level.

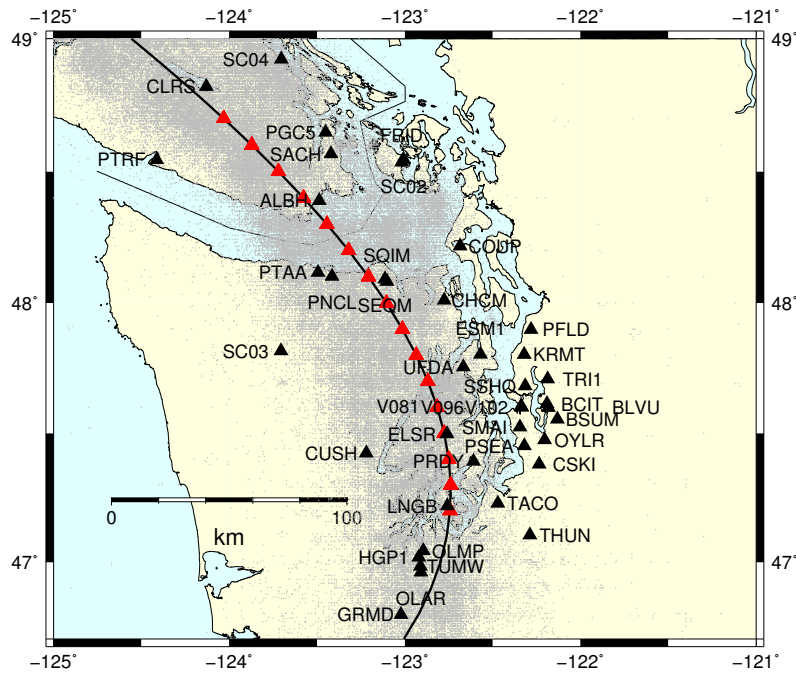


Figure 4: GPS stations used in this study (black triangles). The black line represents the 40 km depth contour of the plate boundary model by Preston et al. [2003]. The red triangles are the locations where we stack the GPS data. The small grey dots are all the tremor locations from the PNSN catalog.

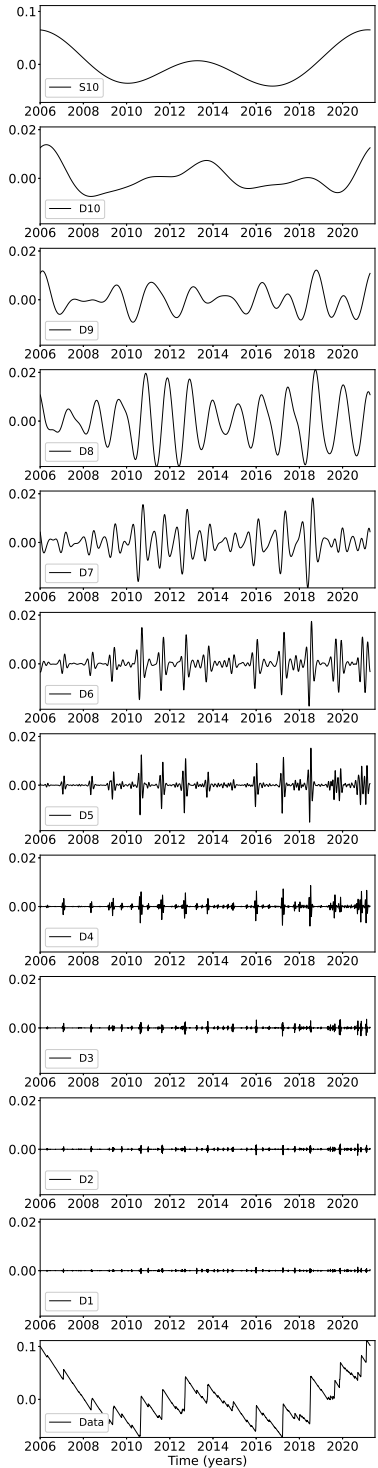


Figure 5: Details and smooth of the wavelet decomposition of the detrended cumulative tremor count around the third northernmost red triangles on Figure 3 (latitude 48.5).

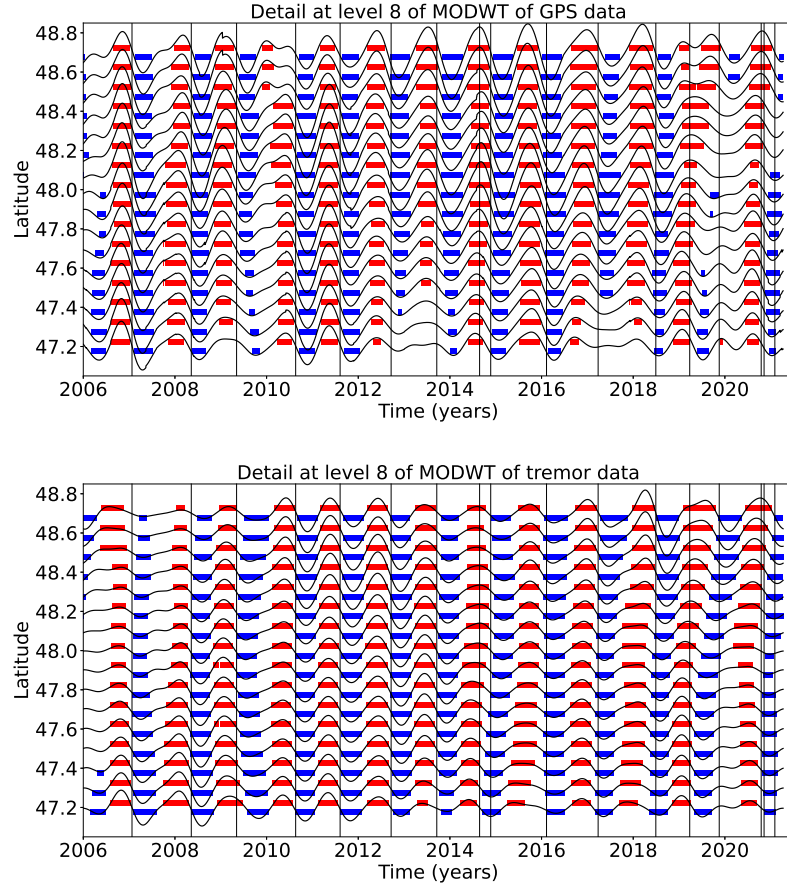


Figure 6: Top: Stacked 8th level details of the wavelet decomposition of the displacement over all the GPS stations located in a 50 km radius of a given point, for the 16 red triangles indicated in Figure 3. Bottom: 8th level detail multiplied by -1 of the cumulative tremor count in a 50 km radius of a given point for the same 16 locations. The black lines represent the timings of the ETS events from Table 1. We mark by a red rectangle every time where the amplitude is higher than a threshold of 0.4 (for the GPS) or 0.003 (for the tremor). We mark by a blue rectangle every time where the amplitude is lower than minus the threshold.

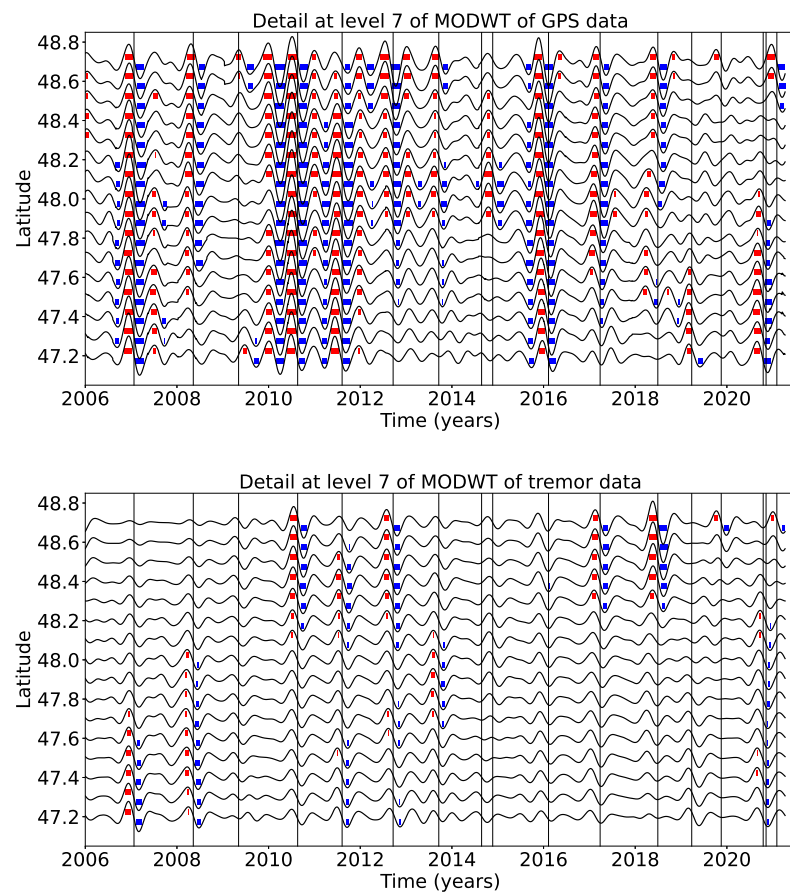


Figure 7: Same as Figure 6 but for the 7th level detail. The thresholds are 0.5 (for the GPS) and 0.01 (for the tremor).

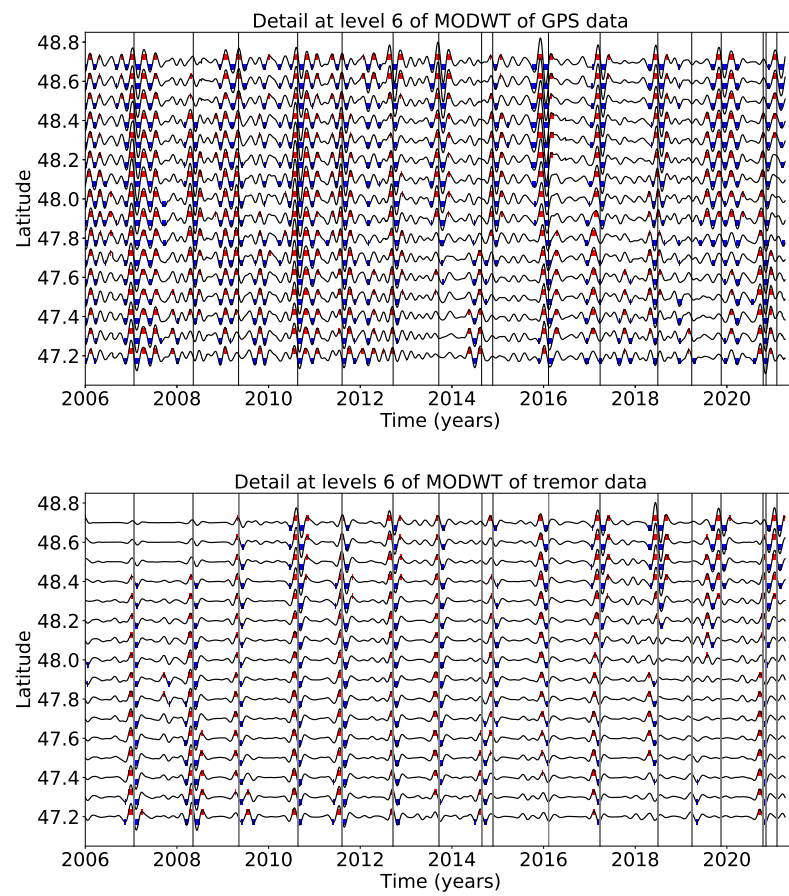


Figure 8: Same as Figure 6 but for the 6th level detail. The thresholds are 0.3 (for the GPS) and 0.009 (for the tremor).

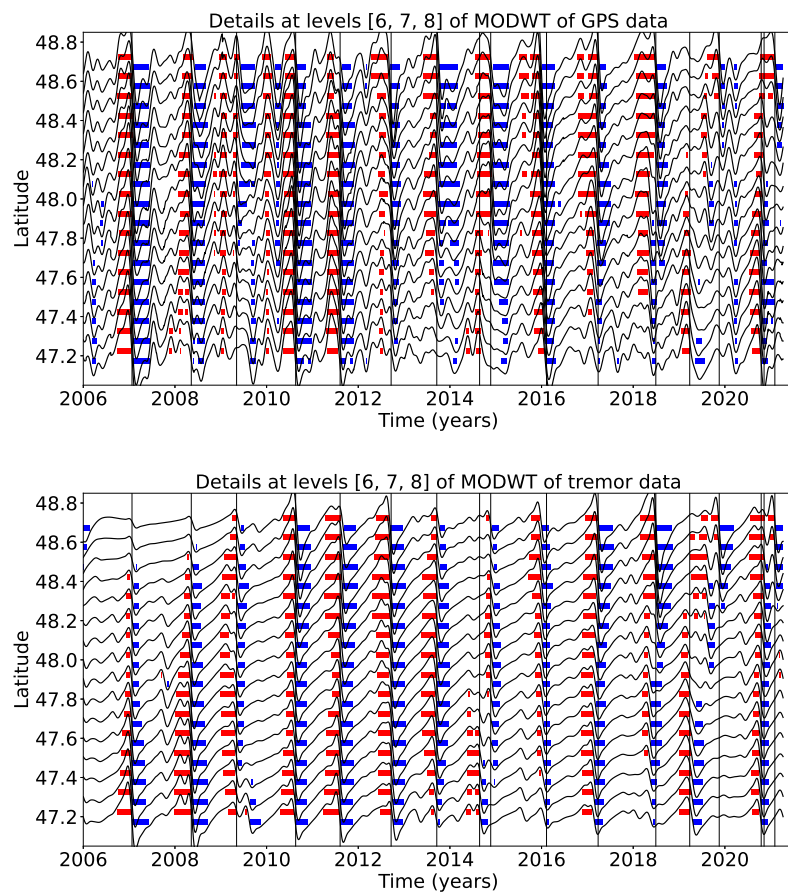


Figure 9: Same as Figure 6 but for the sum of the 6th, 7th and 8th level details. The thresholds are 0.8 (for the GPS) and 0.01 (for the tremor).

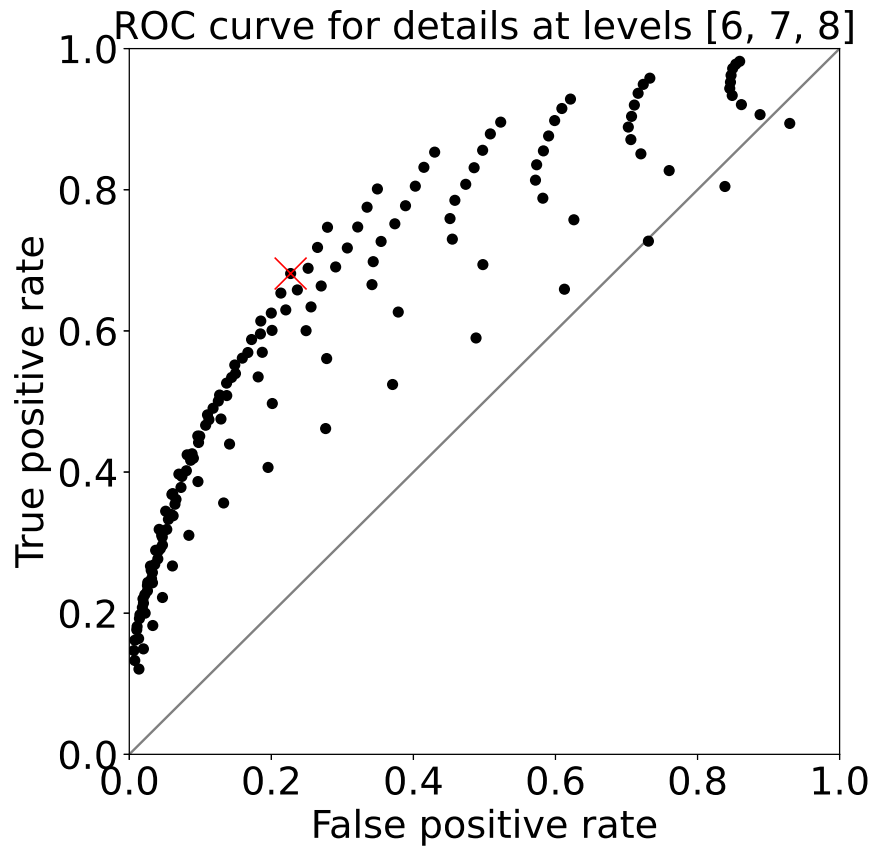


Figure 10: ROC curve for the sum of the 6th, 7th, and 8th level details of the wavelet decomposition. Each black dot represents the true positive rate of event detections and the false positive rate of event detections for a given pair of thresholds (for the GPS and for the tremor). The red cross marks the true positive rate and the false positive rate obtained with the thresholds used to make Figure 9.

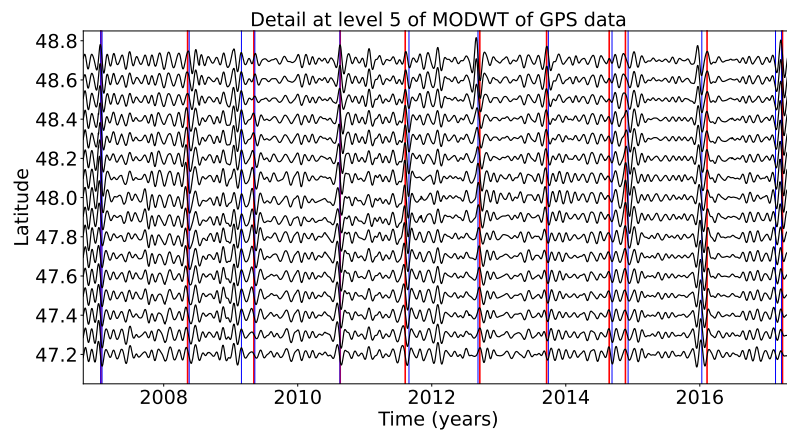


Figure 11: Top: Stacked 5th level details of the wavelet decomposition of the displacement over all the GPS stations located in a 50 km radius of a given point, for the 16 red triangles indicated in Figure 3. The red lines represent the timings of the ETS events from Table 1. The blue lines represent the timings of the magnitude 5 events from the catalog of Michel et al. [2019].